J Mater Sci: Mater Med (2009) 20:51–66
DOI 10.1007/s10856-008-3536-9

On the development of two characteristically different crystal morphology in SiO_2–MgO–Al_2O_3–K_2O–B_2O_3–F glass-ceramic system

Shibayan Roy · Bikramjit Basu

Received: 9 November 2007 / Accepted: 10 July 2008 / Published online: 14 August 2008

Abstract The present work demonstrates how crystals with two different characteristic morphologies can be formed in SiO_2–MgO–Al_2O_3–K_2O–B_2O_3–F glass-ceramic system by adopting two sets of heat treatment experiments. In our study, single stage heat treatment experiments were performed at 1,000°C for varying holding time of 8–24 h with 4 h time interval and as a function of temperature in the range of 1,000–1,120°C with 40°C temperature interval. The constant heating rate of 10°C/min was employed for both sets of experiments. The microstructural changes were investigated using Fourier transformed infrared spectroscopy (FT-IR), SEM-EDS and XRD. For temperature variation batches, the microstructure is characterized by interlocked, randomly oriented mica plates ('house-of-cards' morphology). An important and new observation of complex crystal morphology is made in the samples heat treated at 1,000°C for varying holding times. Such morphology appears to be the results of composite spherulitic-dendritic like growth of mica rods radiating from a central nucleus. The possible mechanism for such characteristic crystal growth morphology is discussed with reference to a nucleation-growth kinetics based model. The activation energy for crystal nucleation and Avrami index are computed to be 388 kJ/mol and 1.3 respectively, assuming Johnson–Mehl–Avrami model of crystallization. Another important result is that a maximum of around 70% of spherulitic-dendritic like crystal morphology can be obtained after heat treatment at 1,000°C for 24 h, while a lower amount (~58%) of interlocked plate like mica crystals is formed after heat treatment at 1,040°C for 4 h.

S. Roy · B. Basu (✉)
Laboratory for Advanced Ceramics, Department of Materials and Metallurgical Engineering, Indian Institute of Technology, IIT, Kanpur, India
e-mail: bikram@iitk.ac.in

1 Introduction

Glass-ceramics typically contain a finite amount of crystalline ceramic phase formed by the controlled crystallization of highly viscous glass-forming melts [1–18]. Glass-ceramics are of interest for various engineering and biomedical applications, because their properties, such as transparency, strength, abrasion resistance, coefficient of thermal expansion can be manipulated over a desired range by tailoring the composition, extent of crystallization, crystal morphology, crystal size and aspect ratio [2–10]. In particular, an important group of these materials, i.e., the mica-containing glass-ceramics received wider appreciation due to their high machinability, which results in an increased versatility of the finished shape, thereby widening numerous possibilities for industrial application [1, 4, 5]. The main crystal phase generated in the K_2O–B_2O_3–Al_2O_3–SiO_2–MgO-F mica system is known as fluorophlogopite having an approximate formula of $K_{1-x}Mg_{3-y}Al_y[(Al,B)_{1+z}Si_{3+z}O_{10+w}]F_{2-w}$, where the total number of anions (oxygen and fluorine ions) must be equal to 12 and remaining parameters are determined as x = 0.01–0.2, y = 0.1–0.2 and w = 0–0.1 [4]. From the crystal structure point of view, it is basically a trioctahedral fluoromica, "composed of 2:1 negatively charged layers that are connected via large, positively charged interlayered alkali (Na/K) ions with a coordination number of 12. A 2:1 sheet consisting of two tetrahedral (T) layers of the composition T_2O_5 (with ½ T = Al and $^3/_2$T = Si)", bonded closely by Mg^{2+} ions in octahedral coordination of $Mg(SiAlO_{10})F_2$" [5].

From the microstructural engineering point of view, a great deal of studies has reported the crystallization behavior of various glass-ceramic materials. For example, Hu et al. investigated the influence of varying amount (0–6 mol%) of ErF_3 doping on crystallization behavior of LaF_3 on oxyfluride glass [6]. Their study suggested a diffusion control growth process in ErF_3 containing glass composition. In a different study, monophase glass-ceramics in SiO_2–Al_2O_3–B_2O_3–MgO–CaO–Na_2O-F system with akermanite phase is designed [7]. The crystallization of akermanite crystalline phase occurs at 700°C or above and the addition of P_2O_5 is reported to increase the stability of glass against crystallization. In the crystallization process of mica based glass-ceramics, the first crystal phase to form at relatively low temperature is called chondrodite, which successively forms norbergite crystals from which the final crystal phase, i.e., fluorophlogopite forms epitaxially. The influence of different fluorine source on the crystallization behavior of R_2O–MgO–Al_2O_3–B_2O_3–SiO_2–F is reported by Cheng et al. [8]. While the addition of NaF is reported to result in precipitation of large dendrite shaped norbergite crystal, plate like fluorophlogopite is formed with MgF_2 addition. Among various studies reporting different crystal morphologies in glass-ceramics [9–18], Hoche et al. reported the growth of highly defective mica plates along with norbergite in an extruded glass-ceramic [9]. In another interesting study, Gebhardt et al. reported the formation of cabbage shaped mica crystal aggregates in micaceous glass system K_2O–Na_2O–Al_2O_3–SiO_2–MgO–F [10].

In the present paper, we will demonstrate how one can obtain unusual combination of spherulitic and dendritic growth morphology of mica crystals with high volume fraction by optimizing the heat treatment conditions in the SiO_2–MgO–Al_2O_3–K_2O–B_2O_3–F glass-ceramic system. This observation is in contrast to earlier reports of either dendritic or spherulitic growth morphology for a given glass composition and it is known that latter is generally feasible at lower temperature and higher viscosity level than the former. In the present study, we report that a combination of both crystallization habits leading to a characteristically different crystal shape is possible when SiO_2–MgO–Al_2O_3–K_2O–B_2O_3–F base glass is isothermally heat treated at 1,000°C. A scientific explanation for the development of such unusual microstructure is also presented. In the present study, critical single stage heat treatment experiments in the varying temperature range of 1,000–1,120°C with 40°C temperature interval for 4 h constant holding time were carried out on the glass-ceramic system. Additionally, experiments at 1,000°C for varying holding time of 4–24 h with 4 h time intervals were also performed. Heating rate remains constant (10°C/min) for both sets of experiments. The microstructural changes of the bulk glass-ceramic samples are observed using optical microscopy, FT-IR (Fourier transformed infrared spectroscopy), SEM-EDS (Scanning Electron Microscope-Energy Dispersive Spectroscopy) and XRD (X-ray Diffraction).

2 Experimental

2.1 Base glass preparation

For our study, the SiO_2–MgO–Al_2O_3–K_2O–B_2O_3–F glass-ceramic system was used and the composition of the base glass was closely related to the commercial composition available in that system (MACOR®, Corning Glass Ltd.). The composition of the starting precursor materials is provided in Table 1. All the starting powders used were of AR (Analytical Reagent) grade chemicals and they were around 99% pure with a very little impurity content. This composition is obtained from the previous work of Guedes et al. [11] and is rechecked from http://www.precisionceramics.co.uk.

Initially, the base glass was prepared at 1,500°C in two steps, i.e., first the frit was prepared by quenching the melt in water and then by subsequently remelting the frit and quenching in air. This procedure is followed and also reported in earlier works for better homogenization of the constituent elements [9, 10, 12]. For frit preparation, the melt was kept at 1,500°C for 1 h and for base glass plate preparation, the holding time was 6 h. For both the cases, the heating rate was 5°C/min and the base glass plate was cooled to room temperature from 1,500°C in 15–20 min. The base glass was optically transparent after melting and no visible

Table 1 Composition of base glass (AR corresponds to analytical reagent grade)

Starting materials	Oxide constituent	Wt.%	Comments
Silica gel in powder form	SiO_2	46	60-120 mesh, AR grade
White tabular alumina	Al_2O_3	16	99.9% pure, $d_{50} < 1$ μm, AR grade
MgO powder	MgO	17	99% pure, AR grade
K_2CO_3	K_2O	10	99.9% pure, AR grade4
Boric acid (H_3BO_3)	B_2O_3	7	99.5% pure, AR grade
NH_4F	F^-	4	95% pure, AR grade

defects in the base glass were observed. It is possible that volatile phases, mainly Silicon tetrafluoride, can evaporate during melting [9]. Such evaporation would reduce the fluorine content in the base glass and in turn, enrich the residual glass with Si, Al and Mg. It has also been reported that this process enables the crystallization of glass to chondrodite stoichiometry, instead of fluorophlogopite [9]. Therefore, it is important to evaluate the volatile loss of glass powder. In the present work, TGA (Thermo Gravimetric Analysis) study (Pyris diamond TGA/DTA analyzer, Perkin Elmer Instruments Technology, USA) up to 1,000°C at 10°C/min heating rate was carried out with the base glass powder. The TGA study showed a weight loss of around 20–25% on heating (see Fig. 1a) and subsequently SiO_2 and NH_4F were added, in excess, to the precursor mix in order to compensate the volatile material loss.

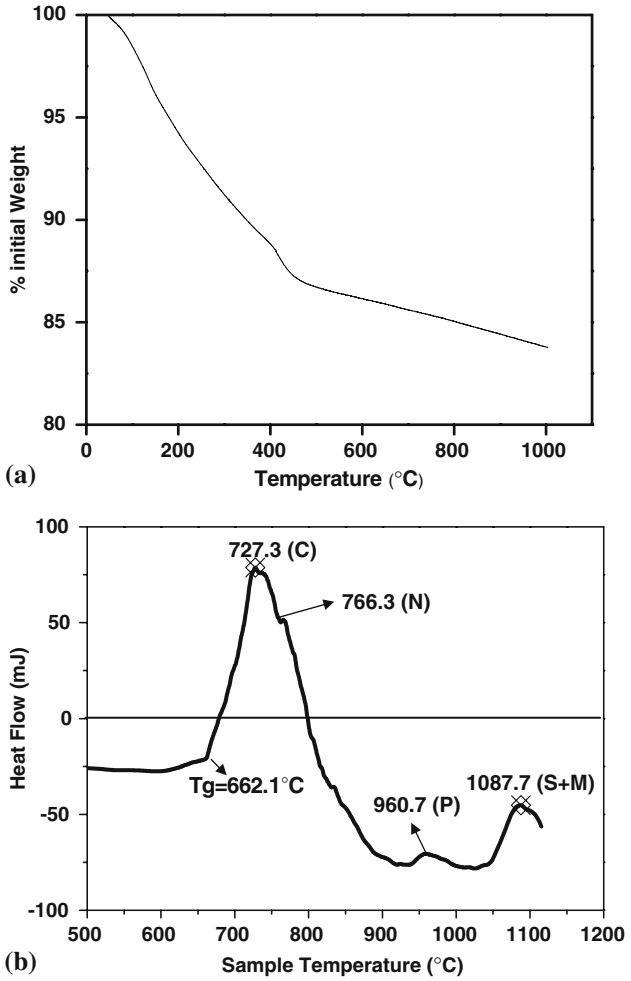

Fig. 1 (**a**) TGA scan of the base glass powder, illustrating the weight loss at 10°C/min heating rate, and (**b**) DTA scan of the base glass (heating rate 17.5°C/min), illustrating the glass transition as well as several phase formation. Various temperatures of interest are also indicated (Tg = Glass transition temperature, C = Chondrodite, N = Norbegite, P = Phlogopite, S = Spinel, M = Mullite). Different peaks in the DTA diagram were identified using the peak identification method in the standard graph plotting software (ORIGIN Inc.)

2.2 Heat treatment experiments

The base glass plate was cut into small pieces of 2.5 cm × 2 cm × 1 cm using a diamond blade cutter (Isomet Low Speed Saw, Buehler, Germany). Three specimens were used for each heat treatment schedule. The crystallization heat treatments were done both by varying temperature from 1,000°C to 1,120°C with 40°C temperature interval for a constant holding time duration (i.e. the holding time at the concerned heat treatment temperature) of 4 h and by varying the holding time duration from 4 h to 24 h with 4 h time interval at constant temperature of 1,000°C. During the heat treatment experiments, the heating rate and cooling rate remained constant at 10°C/min and 3.5°C/min, respectively. It can be mentioned here that most of the previous researchers, e.g., Chen et al. [15], and Gebhardt et al. [10] etc. carried out the crystallization heat treatments in the temperature range of 1,000–1,120°C with almost the same heating rate. A single stage crystallization heat treatment schedule was chosen, as opposed to the classical two stage nucleation-crystallization heat treatments. In the present case, the heating rate is slow and holding time is long enough to promote all the possible nucleation and crystallization processes to occur during the single-stage heat treatment schedule. The reason for keeping the heat treatment temperature in the range of 1,000–1,120°C was that the desired fluorophlogopite phase formed above 900–940°C by the dissolution of norbergite and complete dissolution of norbergite occurs at around 1,100°C [5]. Also, the time variation batch samples were heat treated at 1,000°C for varying time of 8–24 h, because the phase evolution results did not indicate any sign of bulk crystallinity after heat treatment for 4 h and hence it was of interest to investigate the evolution of crystalline phase by providing longer holding time, while keeping the heat treatment temperature constant at 1,000°C.

2.3 Microstructural characterization

After heat treatment, these samples were smoothly polished using diamond paste (from 9 μm to 0.25 μm). The polished surfaces were etched with 12% HF for 5 min to reveal the microstructure. Furthermore, the microstructural characterization of these etched and polished samples was carried out using SEM-EDS (*FEI QUANTA 200, The Netherlands)* and both secondary as well as backscattered electron images were taken. The heat treated specimens was gold coated using a sputtering unit (PS-2 coating Unit, International Scientific Instruments, India) for 5 min. The optical and SEM images were analyzed using Image-Pro-

Plus software for crystal volume fraction calculation. The software was calibrated using a control material with known crystal volume fraction (measured via density determination [1]) prior to the image analysis of the heat treated specimens. At least 25 micrographs of each set of specimens were used for image analysis.

The study of phase assemblage in the heat treated specimens was performed using the XRD *(Isodebyeflex 2002, USA)* technique on the polished surfaces at scan rate of 0.05^{o}/min with a fixed counting time of 3 s. Additionally, Fourier transformed infrared spectroscopy (FT-IR) study of heat treated samples was performed in order to identify the bonding nature as well as the crystalline phases present in the samples. All the microstructural characterizations and phase evaluation studies (XRD and IR spectroscopy) were performed on the bulk of the samples after removing at least 3–5 μm of the surface layer in order to investigate the effect of different heat treatment conditions on the bulk microstructure development. Various JCPDF file numbers: 340158, 100394 and 330853 were used to identify the characteristic XRD peaks for Potassium fluorophlogopite, Mullite ($Al_6Si_2O_{13}$) and $MgAl_2O_4$ spinel phases, respectively. Our FT-IR results were compared with the standard phlogopite (Phlogopite in KBR, CANADA, NMNH 124158) IR spectrum, obtained from the FDM (Fiveash Data Management, Inc.) electronic handbook database.

The density of the heat treated glass-ceramic samples was measured following the Archimedes principle using a laboratory balance and density measurement setup. To investigate the crystallization behavior of the base glass, DTA (Differential Thermal Analysis) *(Perkin Elmer, USA)* was done in the temperature range of 40–1,100°C, with a heating rate of 17.5°C/min. The obtained DTA trace was analyzed after necessary baseline corrections.

2.4 Mechanical and biological characterization

To understand the damage behavior of glass-ceramics having different crystal morphologies, dynamic scratch tests were carried out. The idea of carrying the scratch test was to study the resistance offered by the crystals towards the scratch induced radial/median cracks. Such a study would be helpful to predict the machining as well as the abrasion resistance behavior of glass-ceramic samples. In the present investigation, scratch tests of the heat treated glass-ceramic samples were carried out using a specially designed scratch tester (*TR 101, Ducom, Bangalore, India*), equipped with a conical Rockwell diamond indenter. The details of scratch testing can be found elsewhere [19, 20]. In order to study/simulate the dissolution behavior of the heat treated glass-ceramic material in physiologic environment, the in vitro dissolution study was carried out by immersing selected glass-ceramic samples, both from time variation and temperature variation batches in artificial saliva for four different time periods of 7, 14, 21 and 42 days. The detailed microstructural characterization of the leached surface was performed using XRD and SEM–EDS. The details of in-vitro testing can also be found elsewhere [19, 21].

3 Results

3.1 XRD, FT-IR and DTA data

XRD analysis of the heat-treated samples was carried out in order to identify the crystal phases present (see Fig. 2a). All the temperature variation (representative sample, heat treated at 1,040°C for 4 h) and the time variation batches (representative samples, heat treated at 1,000°C for 4 h and 24 h) show the dominant presence of fluorophlogopite as the main crystalline phase. The sample heat treated at 1,000°C for 4 h did not show any detectable bulk crystal formation, as can be seen from the broad diffuse peak, indicative of the lack of crystallinity and predominant presence of glassy phase. This is further confirmed by SEM images taken from the bulk of the sample (discussed later), where no crystalline phase can be seen and only glassy matrix is visible. Also the XRD analysis of the sample heat treated at 1,120°C for 4 h shows the additional presence of Mullite ($Al_6Si_2O_{13}$) and $MgAl_2O_4$ spinel phases, as opposed to the XRD analysis of other temperature variation samples, which show the presence of fluorophlogopite alone as the principal crystalline phase.

In order to provide complementary information on formation of crystalline phases, FT-IR analysis of some selected samples were carried out and the results are presented in Fig. 2b. A broad IR band in baseline glass sample, spreading over 750–1,500 cm^{-1} with a peak at around 1,034 cm^{-1} indicates the characteristic Si–O stretch band [15]. Such a broad IR band, in well crystallized samples, is replaced by a number of characteristic IR bands (narrow) located at around 1,024 cm^{-1}, near 1,200–1,243 cm^{-1} and closer to 1,600 cm^{-1}. Such IR bands, in combination with additional IR bands (those absent in baseline glass sample), located at $\sim$2,940 cm^{-1} and $\sim$3,265–3,282 cm^{-1} follow closely with the reported IR bands of fluorophlogopite crystals in the SiO_2–MgO–Al_2O_3–K_2O–B_2O_3–F glass-ceramic system, as also reported in Ref. [1]. Our experimental IR results are also comparable with that of the standard phlogopite (Phlogopite in KBr, Canada, NMNH 124158) spectrum obtained from FDM electronic handbook database. FT-IR results therefore reconfirm the presence of phlogopite as the principal crystalline phase in both 'temperature variation' and 'time variation' samples.

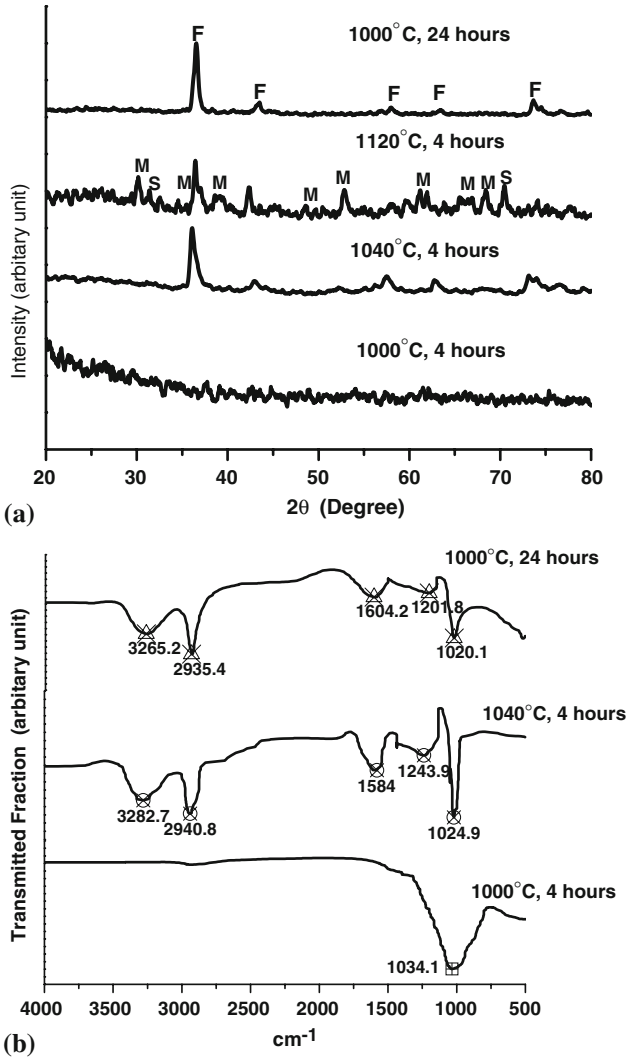

Fig. 2 (**a**) XRD spectra taken from the polished surface at the bulk of the heat treated samples ('F' stands for Fluorophlogopite, 'M' for Mullite and 'S' for spinel), and (**b**) IR spectrum of heat treated samples. Sample heat treated at 1,000°C for 4 h represents the base glass characteristics. Similarly, samples heat treated at 1,040°C for 4 h and 1,000°C for 24 h represent the temperature and time variation batches containing the maximum volume fraction of crystalline phase, respectively. Both the phase analysis results show the presence of phlogopite as the main crystalline phase for all the heat treated samples

In an effort to capture the thermally induced stages of crystallization, a representative DTA plot of the glass-ceramic powder mix is presented in Fig. 1b. During non-isothermal heating of a glass-ceramics, a sequence of thermal effects, e.g., structural relaxation, glass transition, softening and nucleation and crystallization is realized over the transformation temperature range. The characteristic slope change of DTA curve (see Fig. 1b) in the vicinity of 662°C can be attributed to the glass transition temperature (T_g). Above T_g, the glass undergoes various transformation events, involving changes in heat capacity and other property change, which together lead to the inflexion point at the slope change in DTA curve. Furthermore, the appearance of a strong exothermic asymmetric peak in DTA plot, at ~727°C, indicates the crystallization process. It can be noted that T_g is around 650°C and the exothermic peak maximum occurs at around 750–825°C for Dicor® glass composition [22]. The large exothermic peak at ~727°C accounts for the chondrodite formation (see Fig. 1b), whereas the successive undulation at ~766°C is presumably due to the formation of norbergite. The observation of endothermic peaks above 900°C (at ~960°C) accounts for the formation of fluorophlogopite by the dissolution of norbergite. The endothermic peaks, appearing at around 1,090–1,100°C (at ~1,087°C), possibly result from the evaporation of volatile silicon tetrafluoride from the base glass during heating and subsequent dissolution of fluorophlogopite to form additional phases like Mullite and $MgAl_2O_4$ spinel [9].

3.2 SEM-EDS analysis of heat treated glass-ceramics

The detailed microstructural analysis by electron microscopy technique of different heat-treated samples at varying temperature as well as varying time is presented in Figs. 4–6. The samples heat-treated at 1,000°C for 4 h show no sign of detectable bulk crystal formation (see Fig. 3a). However, the samples heat treated at 1,040°C, 1,080°C and 1,120°C for 4 h show the usual microstructure of straw like interlocked mica flakes, randomly oriented in the glassy matrix (see Fig. 3b, c, and d). The characteristic features include a width of 1–1.5 μm, average length of 10–15 μm and interlocking crystal arrangement. The interlocking nature is more visible in Fig. 3e, which shows the connectivity of the mica rods. SEM-EDS analysis reveals the strong presence of Si with moderate and comparable intensity peaks of Mg and Al in the crystalline phase (see Fig. 3f). Also, for the sample heat treated at 1,120°C for 4 h, a needle shape is observed at the end of mica plates (see Fig. 3e). This 'straw' like morphology of the characteristic mica crystal phase and the randomly oriented, interlocked microstructure is known as 'house of cards' microstructure, reported also by previous researchers, e.g., Habelitz et al. [23] and Höche et al. [5]. Other characteristic morphology is also reported. For example, Vogel et al. [4], Gebhardt et al. [10] and Höland [24] reported a "Cabbage" shaped morphology in a slightly different base glass composition (21.2 mol. % MgO, 19.5 mol. % Al_2O_3, 59.3 mol. % SiO_2 doped with 11.2 mol. % F^- and 6.4 mol. % Na_2O/K_2O) and at a heat treatment temperature lower than 1,000°C. Any other morphology of fluorophlogopite is not reported yet.

In this context, the morphology of the crystal phase in time variation samples is quite interesting. The

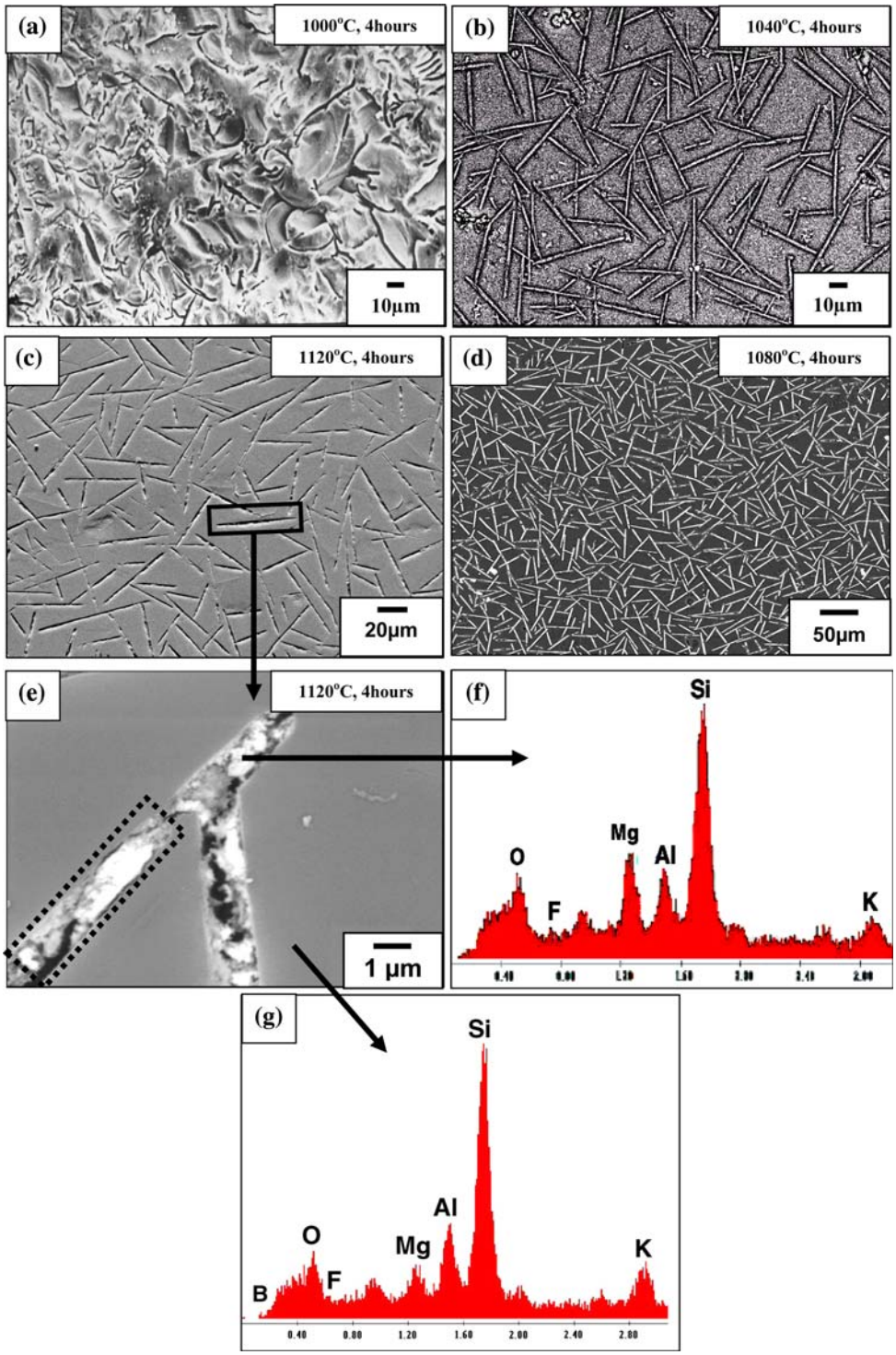

Fig. 3 SEM micrograph of samples heat treated at (**a**) 1,000°C, 4 h, showing no sign of crystallinity, (**b**) 1,040°C, 4 h, (**c**) 1,080°C, 4 h, and (**d**) 1,120°C, 4 h showing usual randomly oriented interlocked mica flake, (**e**) 1,080°C, 4 h showing the interlocking between individual mica flakes and a characteristic needle shape (possible sign of mullite formation) at the end of the mica rods; the rod like mica crystal appears as rectangular plate in two dimension, which is being shown with dotted line in the micrograph, (**f**) corresponding EDS spectrum of the characteristic crystal phase, and (**g**) corresponding EDS spectrum of the characteristic glassy matrix phase. The first micrograph is a secondary electron image; rests are all backscattered electron images

microstructural evolution of samples heat-treated at 1,000°C for varying time period is presented in Fig. 4. The important observation is that a typical crystalline morphology with a number of mica rods radiating from a central nucleus constitutes as the major microstructural phase (see Fig. 4a). Such morphology of the crystal phases is common for all the time variation batches, i.e., samples heat treated at 1,000°C for 8, 12, 16, 20 and 24 h. At the end of each of the mica rods, a characteristic 'tree leave' shaped structure is seen (see Fig. 4e). Small fragments of mica plate are found to be scattered all over the crystal phase (see Fig. 4f). Closer observation of Fig. 4h reveals the stacking of mica plates in the formation of mica rods. In the sample heat-treated for 24 h, the characteristic crystal

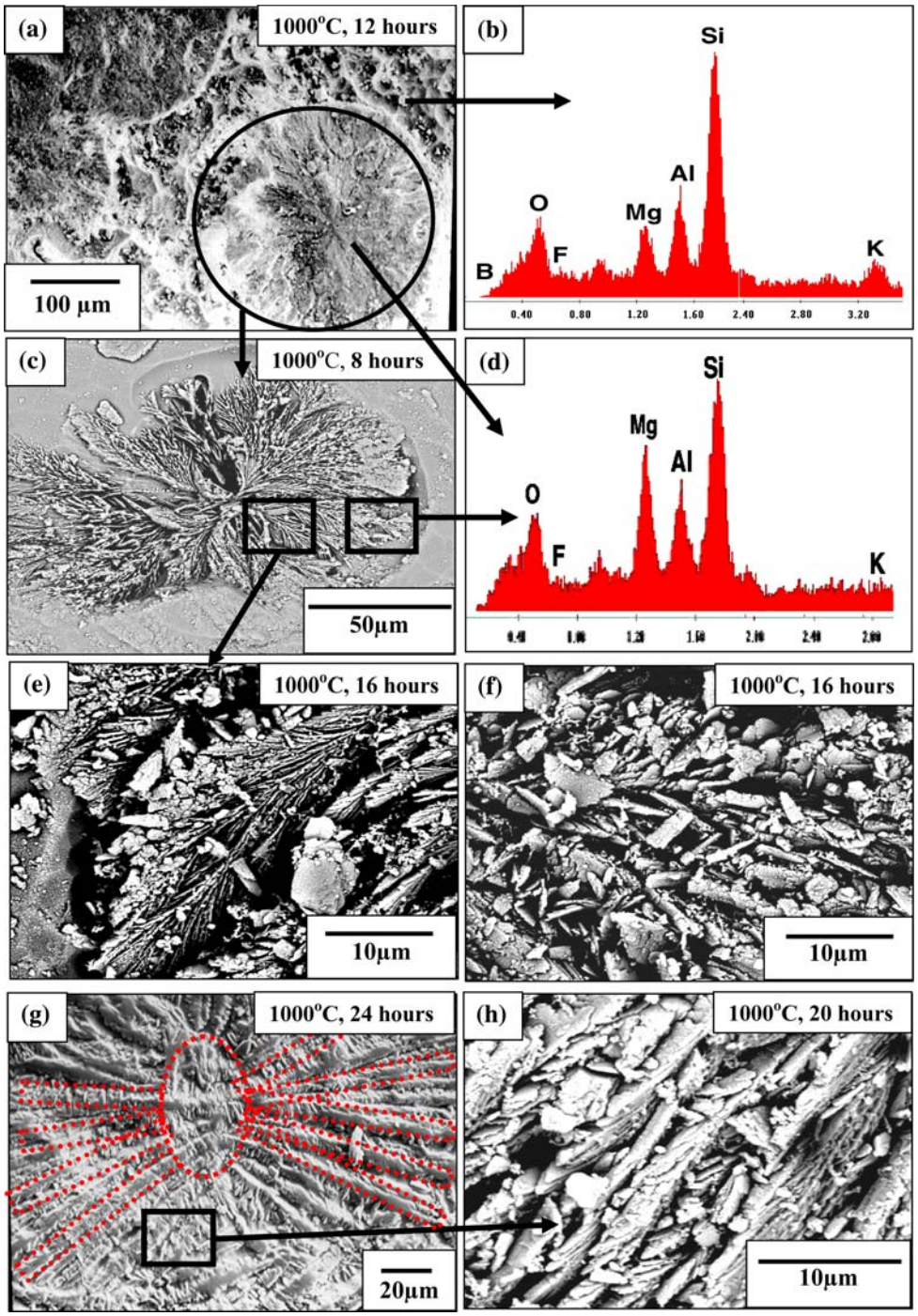

Fig. 4 SEM micrographs of time variation samples heat treated at 1,000°C showing (**a**) Crystals evolved from spherical droplets (Holding time 12 h), (**b**) corresponding EDS spectrum of the glassy matrix phase, (**c**) single "Butterfly" shaped crystals (Holding time 8 h), (**d**) corresponding EDS spectrum of the crystal phase (**e**) "Tree leave" structure at the end of each mica rod (Holding time 16 h), (**f**) Scattering of mica plates over the crystal phase (Holding time 16 h), (**g**) Individual butterfly crystal showing different length of different crystals; the 'butterfly' like shape (central nucleus and individual mica rods elongated from this nucleus) is shown with dotted lines (Holding time 24 h) and (**h**) Stacking of mica plates forming mica rods (Holding time 20 h). The first micrograph is a secondary electron image; rests are all backscattered electron images

morphology with radiating mica rods from the central nucleus is clearly visible (Fig. 4g). In the time variation batches, the crystal phases seem to be formed in some localized regions with large amount of spacing between each other for lower holding time of 8, 12 or 16 h. As the holding time increases (20 h and 24 h), more and more such crystals are formed in different regions with narrower spacing and seemed to overlap so that the glassy matrix is confined within a small isolated region (see Fig. 5a). The samples heat treated up to 24 h show the maximum crystallization among all the time variation batches as well as among all the other heat treated samples (see Fig. 5b). It can be noted here that Henry et al. [9] also observed similar effect of increased isothermal holding time, which resulted in high degree of connectivity of the potassium fluorophlogopite phase for an almost identical glass-ceramic composition. The compositions of the glass matrix surrounding the crystal phases are however identical for

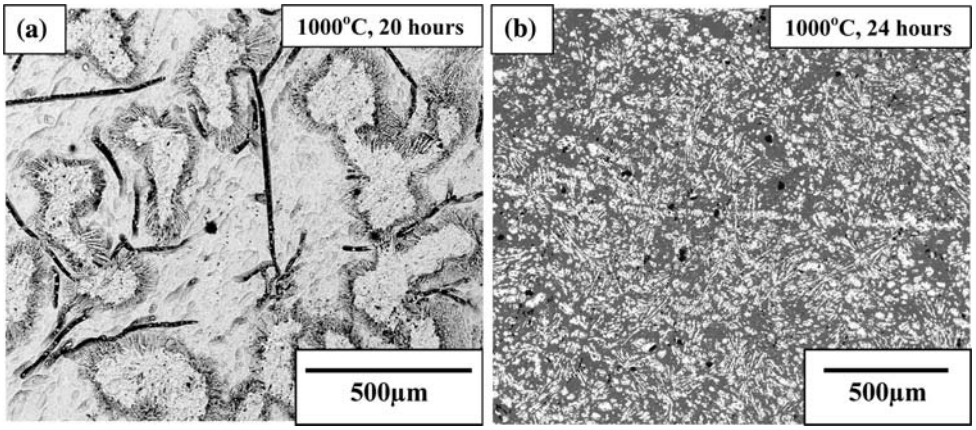

Fig. 5 SEM micrographs of time variation samples heat treated at 1,000°C showing (**a**) overlapping of crystal phases for 20 h holding time sample and (**b**) confinement of glassy matrix within small isolated regions after heat treatment for 24 h (crystal volume fraction 70%)

both temperature and time variation batches (see Fig. 3g and 4f). It is evident that the relative proportion of Si in glassy matrix is much higher than that in the crystal. As reported in literature, the matrix is basically potassium alumino-borosilicate glass enriched with K_2O, B_2O_3, Al_2O_3, MgO and SiO_2 [30]. In view of such observations, the residual glass is silica rich, however exact composition cannot be obtained from SEM-EDS analysis.

The compositional analysis of different crystalline phases is performed using SEM-EDS in order to find out compositional variation. The line scans are performed on an individual Spherulitic-dendritic crystal; both along the vertical direction as well as along the width of the crystal, the accusation time at each point for both the directions being 4,000 milliseconds (see Fig. 6). In both the directions, it has been observed that the relative intensity of Si is sharply increased at a distance of around 50 µm from the central point. These observations are shown in Fig. 6b and c. Additionally, this trend of the relative intensity change of Si is comparable in both the sides of the central nucleus.

As far as the phenomenology of crystal growth in glass matrix is concerned, it is known that if the glass is significantly undercooled or crystallizes initially to a phase with different composition, two types of fibrilar or skeletal type of crystallization habits are resulted [25]. The dendritic morphology is normally referred to as tree-like or sheaf-like

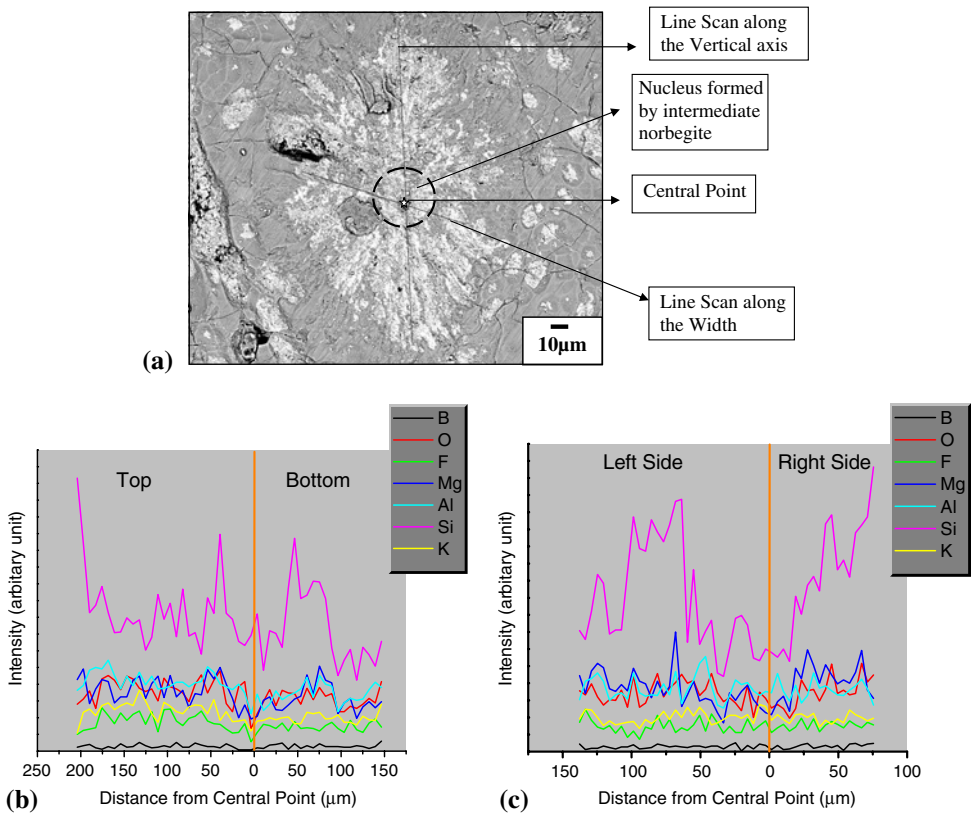

Fig. 6 (**a**) SEM image of an individual butterfly crystal showing the positions of line scans. (**b**) X-ray intensity variation during line scan using SEM-EDS along the vertical axis of the crystal, and (**c**) along the width of the crystal

Table 2 Different crystal shapes formed in various amounts by different crystallization heat treatment experiments (Crystal volume fraction corresponds to the fluorophlogopie crystals only)

Heat treatment condition	Crystal morphology	Crystal volume fraction (%)
1,000°C for 4 h	No detectable bulk crystallization	–
1,040°C for 4 h	Random, "Straw" like	59.2
1,080°C for 4 h	Random, "Straw" like	46.1
1,120°C for 4 h	Random, "Straw" like	46.8
1,000°C for 8 h	Random, "Butterfly" shaped	26.3
1,000°C for 12 h	Random, "Butterfly" shaped	39.0
1,000°C for 16 h	Random, "Butterfly" shaped	52.3
1,000°C for 20 h	Random, "Butterfly" shaped	54.3
1,000°C for 24 h	Random, "Butterfly" shaped	70.1

crystals with significant branching, whereas spherulitic morphology describes the formation of sub-parallel needle-like crystallites radiating from a distinct nucleus, which form essentially a spherical shaped crystal phase. For both types of crystal habits, the crystal growth usually proceeds more rapidly in certain lattice directions and this result in the development of dendritic or spherulitic arms [25]. In the above backdrop, the characteristic crystal morphology developed in the 'time variation' batch samples cannot be completely described solely by either of the growth morphologies and in contrast, can be better described by a composite spherulitic-dendritic like growth morphology and hence, we call them as 'spherulitic-dendritic' crystals.

Table 2 summarizes the details of crystals shape formed and the amount of crystal phase generated in different heat treated samples. The crystal volume fraction of all the batches is measured using the image analysis of the micrographs taken by both the optical and electron microscope. For the 1,000°C, 4 h samples, the volume fraction of the crystals cannot be measured as it is completely glassy without any detectable sign of crystal formation. For other samples of temperature variation batches, glass-ceramic heat treated at 1,040°C for 4 h shows the maximum crystal phase formation of more than 55% by volume, whereas the other two batches, i.e., samples heat treated at 1,080°C and 1,120°C for 4 h, show lesser amount of crystal formation of around 45–48%. The crystal volume fraction in the two batches heat treated at 1,080°C and 1,120°C for 4 h are almost comparable (see Fig. 7a). For time variation samples, however, crystal volume fraction varies almost linearly in a wide range from nearly 20% for 8 h holding time sample to nearly 70% for 24 h holding time sample (see Fig. 7b). Such a linear increase in crystallization with time, as observed with spherulitic-dendritic morphology, is consistent with crystal fibrils always moving into the surrounding glass of constant composition or with the fibrils growing under steady state conditions with a constant radius of curvature at the growth front [25].

The variation in the crystallization of the glass-ceramic samples can also be assessed from the density measurements. Figure 8 plots the density variation of the heat treated samples. From thermodynamic point of view, a stable crystal, in a glass-ceramic system, has lower free energy and higher density than an unstable amorphous phase with the same composition. Consequently, the density of the glass-ceramic samples is much higher than the original parent glass and such density difference is an effective way to find out the amount of crystalline phase, as was demonstrated by Karamanov and Pelino [2]. In case of temperature variation samples, the crystal volume fraction of the temperature variation samples follows almost the same order of density (see Fig. 8a) and a maximum density occurs for sample heat treated at 1,040°C for 4 h (~2.65 gm/cc). On the other hand, for the time variation samples, density is highest (~2.65 gm/cc) for the sample heat treated at 1,000°C for 24 h containing the highest amounts of crystalline phase in the glass matrix (~70%) and lowest (~2.50 gm/cc) for the sample heat treated at 1,000°C for 4 h. It can be mentioned here that the density of the commercial MACOR® glass-ceramics based on the SiO_2–MgO–Al_2O_3–K_2O–B_2O_3–F glass-ceramic system is 2.52 gm/cc (http://www.precessionceramics.co.uk), which

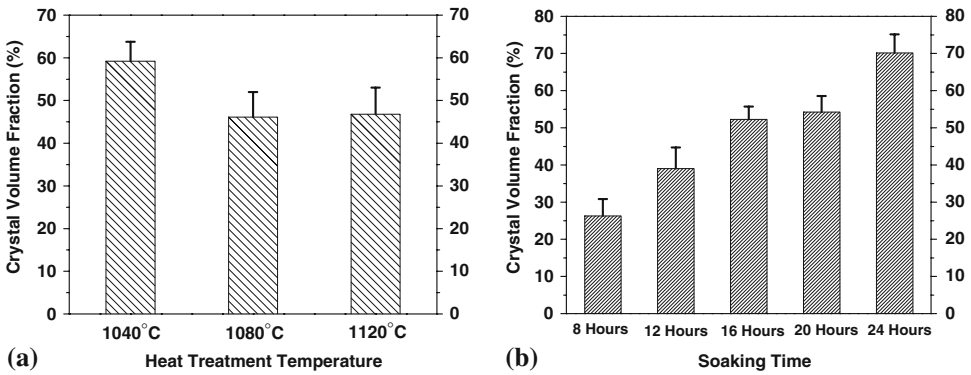

Fig. 7 Plot of crystal volume fraction in glass-ceramic samples (**a**) heat treated for 4 h at various temperatures (1,000–1,120°C) and (**b**) heat treated for various holding time (8–24 h) at 1,000°C. It can be noted here that no crystallization was noticed for sample heat treated at 1,000°C for 4 h

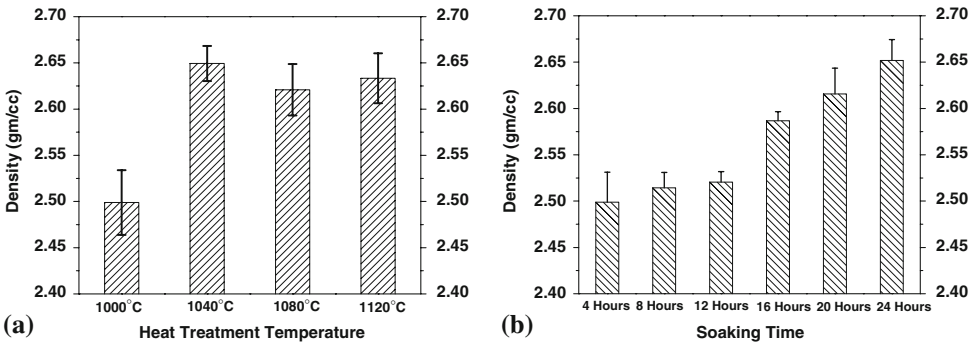

Fig. 8 Density variation of heat treated samples measured by the Archimedes principle using a laboratory balance and density measurement setup, (**a**) temperature variation samples, and (**b**) time variation samples

means the glass-ceramics prepared in the present study, has a higher density than the commercial product.

4 Discussion

4.1 Microstructure development

Summarizing the experimental results, two characteristics microstructural morphology, i.e.,'straw' like and composite 'spherulitic-dendritic' like crystalline phases are formed for identical base glass composition during the two separate sets of heat treatment schedules, i.e., temperature variation (1,000–1,120°C, 4 h) and time variation (1,000°C for 8–24 h), respectively. In explaining the growth morphology, it is important to realize the similarity as well as differences in the growth mechanism of two types of crystal morphology. In both cases, the normal growth with volume crystallization mechanism, in contrast to surface crystallization, took place. However, in the case of 'house-of-cards' morphology, anisotropic crystal growth involving preferred orientations with higher growth rate occurs. For spherulitic-dendritic growth morphology, primary growth process, characterized by "growth to impingement" occurs.

Such a difference in crystal morphology can be explained on the basis of difference in crystallization and growth mechanisms. In the crystallization process of SiO_2–MgO–Al_2O_3–K_2O–B_2O_3–F system, a spinoidal phase separation occurs first, due to the presence of fluorine and small droplets of an F-rich potassium alumino-borosilicate glass phase are formed. The matrix phase is enriched with K_2O, B_2O_3, Al_2O_3, MgO and SiO_2. The primary crystallization involves the formation of dendritic chondrodite, at the interface between the two liquid phases, as a solid solution with composition of $2Mg_{2-x}(Al,B)_{2x}Si_{1-x}O_4 \cdot MgF_2$, where $x \approx 0.15$ [4, 8]. Subsequently, the recrystallization occurs in the temperature range of 750–900°C with the formation of norbergite [$Mg_2SiO_4 \cdot MgF_2$] crystalline phase, which helps in the epitaxial growth of main crystalline phase fluorophlogopite at higher temperature (above 900°C) [6]. $MgAl_2O_4$ spinel phase may also form along with fluorophlogopite above 1,100°C for a prolonged period of heating [23]. There exists a structural similarity between the (100) plane of norbergite and the (002) plane of fluorophlogopite. In particular, the difference in lattice parameters is limited to less than 5%. This eventually makes epitaxial interaction possible [4]. Because of their three-layered structure, mica crystals feature pronounced preferential growth along the (001) plane, as this is the most loosely packed plane in the structure. The anisotropic growth results in the formation of mica plates or rather 'straw' like morphology in the temperature variation batches. The overlapping of different mica rods, starting from different norbergite crystals and growing in different directions, causes the interlocking of these mica plates. Although, DTA scan of the base glass reveals the crystallization temperature of fluorophlogopite to be around 900–940°C (see Fig. 1b), the samples (heat treated for 4 h at 1,000°C) do not produce any crystal in the bulk of the sample as is evident from the XRD study (see Fig. 2a) and SEM observations (see Fig. 3a). It is also likely that the temperature or holding time is not sufficient to initiate bulk crystal formation in the sample heat treated at 1,000°C for 4 h as the crystallization in a glass-ceramic requires activation energy, i.e., sufficient thermal energy input to initiate crystal formation. Another important consideration is that the DTA was performed on a powder sample where the temperature would not have the same profile as that of the massive, bulk glass-ceramic samples. This could lead to a difference in the number of possible nucleation sites available for crystallization and subsequently the presence of crystals at a particular temperature for the powder and the bulk samples.

In the following, we will make an attempt to analytically compute the activation energy of crystallization. Among many theoretical models available, the most widely used John-Mehl-Avrami (JMA) equation [26, 27] has been used to determine the activation energy for isothermal crystallization of 'Spherulitic-dendritic' shaped crystals:

$$-\ln(1 - x) = (Kt)^n \quad (1)$$

where x is the crystallized fraction, t is the crystallization time, n is reaction order or Avrami

index; and k is a constant, which can be expressed by Arhenius equation,

$$k = \upsilon \exp(-E_c/RT) \quad (2)$$

where T is the absolute temperature of crystallization, E_c is the activation energy of the crystallization and v is the frequency factor.

Based on the experimentally measured values, as also plotted in Fig. 7b, the value of 'n' is computed to be 1.3 (using Eqs. 1 and 2). Such low value of 'n' indicates that the crystallization, in the present case occurs by the process of diffusion-controlled transformation, which involves initial growth of particles nucleated only at start of transformation [28]. According to Clupper and Hench, such low value of n (≈ 1) can be explained by a slow nucleation on the surface and infinitely rapid growth of the nuclei [29]. It can be mentioned here that much higher value of $n = 3.4$ is reported for nucleation and crystallization of tetrasilicic fluormica crystals in Dicor® glass-ceramics [22]. In general, $n = 4$ is for continuous, homogeneous nucleation, whereas $n = 3$ is generally observed for fast heterogeneous nucleation [30]. Additionally, the activation energy for crystallization, in the present case, is calculated as 388 KJ/mol. In the above calculation, the frequency factor is assumed as 2.88×10^{11} sec^{-1}, as reported elsewhere for glass-ceramic system SiO_2–MgO–K_2O–F [22]. For phologopite crystals in SiO_2–Al_2O_3–MgO–Na_2O–K_2O–F glass-ceramic system, little lower activation energy of 314 kJ/mol [31] and even lower activation energy of 280 kJ/mol are reported for 45S5 glass ceramics [32]. Also, lower activation energy of 203 kJ/mol was recorded for crystallization of Dicor® glass-ceramic system in the temperature range of 750–880°C. Much higher activation energy for bulk crystallization of spherulitic-dendritic crystals is consistent with our observation that a holding time of 4 h at 1,000°C is not sufficient to initiate crystal formation in the present case.

From the above analysis, it is clear that an incubation time of more than 4 h at 1,000°C is required for the crystallization to occur in this glass-ceramic system in a single stage heat treatment schedule. It can be noted here that Henry and Hill [33] made a similar observation in a BaO and Li_2O containing potassium fluorophlogopite {$3Al_2O_3$–$8SiO_2$–(3–S)MgO–$3MgF_2$-(1–Z)BaO–ZK_2O–SLi_2O} glass-ceramic system. It was reported that when $S = 0.5$ and $Z = 1$, holding at 1,000°C for 1 h does not produce any definable crystalline microstructure, whereas a longer holding time of 3–5 h produces crystals in the same glass composition [33].

As the heat treatment temperature increases from 1,000°C to 1,040°C, crystals start forming at the bulk of the samples and reaches to a maximum volume of nearly 58%. Further increase in heat treatment temperature do not increase the amount of crystal formation, rather the existing crystals with an aspect ratio of <1 get dissolved and eventually deposited on the already present larger crystals, so that the aspect ratio of crystals increase in lieu of overall crystal volume fraction in samples, heat treated at 1,080°C and 1,120°C for 4 h (see Fig. 4b, c, and d). This process is quite similar to the widely reported Oswald ripening process in metals and is earlier observed by other researchers, e.g., Henry and Hill [33] and Grossman [34]. XRD analysis of the sample heat treated at 1,120°C for 4 h shows the presence of Mullite and $MgAl_2O_4$ spinel peaks (see Fig. 2a). Also, the needle shape formed at the end of the mica plates (see Fig. 3e) is likely to be Mullite crystals, heterogeneously nucleating over the pre-existing fluorophlogopite crystals. Similar observation was made in earlier studies when the heat treatment temperature exceeded 1,100°C [23, 33]. The formation of these secondary phases at higher temperature (>1,100°C) is possibly related to the volatilization of silicon tetrafluoride, resulting in the subsequent dissolution of fluorophlogopite crystals and the enrichment of the remaining glassy phase with alumina, silica and magnesia [33].

The microstructure of glass-ceramics, heat treated for varying time periods at 1,000°C, provides different set of information. If, sufficient time is provided, the set of SEM images in Figs. 5 and 6 implicate that epitaxial growth may occur from other crystallographic planes of a preexisting norbergite. Subsequently, it is possible that the mica rods can be generated in all directions from the central nucleus of norbergite crystals. This phenomenon can eventually lead to the formation of the characteristic 'Spherulitic-dendritic' morphology, as obtained in time variation batches. The probable reason for the occurrence of the unique morphology, i.e.,'spherulitic-dendritic' shape of fluorophlogopite is related to the mechanism of crystal phase formation in SiO_2–MgO–Al_2O_3–K_2O–B_2O_3–F system. As revealed in EDS analysis, the presence of higher amount of Mg in spherulitic-dendritic crystals, as compared to that in 'straw' like crystals, also suggest that more amount of norbergite, is transformed to phlogopite during the formation of these spherulitic-dendritic crystals. Norbergite is a solid solution of Mg_2SiO_4 and MgF_2, which means that it contains relatively greater concentration of Mg, Si, O and F, compared to fluorophlogopite. The increase in the relative intensity of Si very near the central point clearly suggests that the nucleus (as shown by the dashed line in Fig. 6a) is composed of intermediate norbergite, over which fluorophlogopite starts growing. Also, a similar trend in Si intensity variation on the two sides of the central point, both along the vertical direction as well as along the width of the characteristic 'Spherulitic-dendritic' crystal, suggests that the fluorophlogopite mica rods or plates are formed in all possible directions from the central nucleus of intermediate norbergite crystal.

The multi-directional growth of crystal planes from the central nucleus will now be explained. According to Reed-Hill [35], the crystallographic planes having higher "accommodation factor", i.e., loosely packed planes have a faster growth rate than comparatively close packed planes during crystal growth. However, the growing crystals do not necessarily assume only the faces of these loosely packed planes. On the contrary, with increasing time, the tendency for the crystals is to assume faces that are close packed, or slow growing. This is because of the fact that the low density planes, having faster growth rate, tend to grow themselves out of existence, leaving behind only close packed surfaces. At 1,000°C, some of the intermediate norbergite crystals start forming phlogopite along the preferred <001> direction with faster speed. Crystal growth also starts from some other closely packed planes, but at a much slower speed. For a long holding time of 8 h, sufficient growth of mica rods occurs in some directions other than the most preferred <001> direction so that the spherulitic-dendritic crystals with difference in length of the constituent mica rods are formed. This can be seen in Fig. 6a, where an individual spherulitic-dendritic crystal is being shown. It is interesting to observe that the central rods formed from both sides of the nucleus are the longest one with a length of about 150–200 μm, whereas the other nearby mica rods formed from the same nucleus are comparatively smaller than the central one. The above mentioned physical growth process continues for other time variation batches also, where more and more initial norbergite starts forming mica plates with increasing holding time. This eventually results in overlapping of different spherulitic-dendritic crystals. These phenomena are believed to result in almost linear increase of the crystal volume fraction in time variation batches (see Fig. 7b).

As far as the alternative explanation for the 'spherulitic-dendritic' crystal is concerned, it is quite possible that for a sufficiently longer period of time, heat dissipation through the glass matrix can bring down the temperature difference between the glass matrix and the crystal-glass interface. Simultaneously, the concentration of the base glass, surrounding the crystals, increases radially along the interface due to the anisotropic growth of the mica rods. According to Avramov and co-workers [36, 37], the linear growth rate (G) of crystals generally obey the following relationship,

$$G = \frac{cd_0}{\eta}\omega\left[1 - \exp\left(-\frac{\Delta\mu}{RT}\right)\right] \tag{3}$$

where d_0 is the interatomic distance, c/η (η—viscosity) accounts for the frequency at which molecules cross the interface, ω is a parameter accounting for the mode of growth and $\Delta\mu$ denote the supersaturation.

The supersaturation can be further expressed as,

$$\Delta\mu = \Delta\mu_T - \Delta\mu_d - \Delta\mu_c \tag{4}$$

where $\Delta\mu_d$ accounts for the existence of the large number of defects in growing crystals, while $\Delta\mu_c$ is attributed to the difference in chemical composition. As a first approximation, $\Delta\mu_T$ depends on the temperature,

$$\Delta\mu_T = \Delta H_m \frac{[T_m - T]}{T_m} \tag{5}$$

where ΔH_m is the melting enthalpy and T_m is the melting point.

In Eq. 3, the rate controlling parameters are both viscosity (η) and supersaturation. As far as relative contribution of various components to $\Delta\mu$ is concerned, we believe the radial compositional gradient from the central nucleus towards untransformed glass matrix favors the multi directional growth in case of 'spherulitic-dendritic' crystals. For longer holding time, more dissolution of norbergite occurs and consequently, matrix composition (slightly Mg-rich) is restored. This will eventually lead to the dendritic crystal growth at the sides as well as at the edges of each of the mica rods. The dendritic growth and subsequent branching will lead to the characteristic 'tree leave' structure at the end of each of the mica rods of the spherulitic-dendritic crystals. This is also the reason for the scattering of small fragments of mica plates all over the spherulitic-dendritic crystals. In temperature variation batches, the comparatively smaller holding time of 4 h, probably, is not sufficient to cause any dendritic growth or branching at the end of each mica rod.

These two different crystallization mechanisms in temperature and time variation batches are schematically shown in Figs. 9a and b, respectively. For temperature variation batches, at the beginning, fluorophlogopite starts forming from norbergite. With increasing time and temperature, the anisotropic growth of these early fluorophlogopite crystals leads to single rod formations (see Fig. 9a). This continuous growth will cause overlapping or rather interlocking of these mica rods and subsequently, after 4 h, a network of randomly oriented, interlocked, 'straw' like crystals would be obtained. On the other hand, for time variation batches (see Fig. 9b), fluorophlogopite starts forming from norbergite epitaxially as earlier, but most importantly, with increased holding time, mica rods start forming in other directions also at a much slower rate (see Fig. 9b). This will again cause overlapping, when the holding time is just enough to produce higher volume fraction of crystals and a network of 'spherulitic-dendritic' like crystals is formed. The point to be noted here that for the usual rod shaped crystal containing mica glass-ceramic materials, the process of dissolution of the existing crystals and eventual deposition on the already present larger crystals, increases the aspect

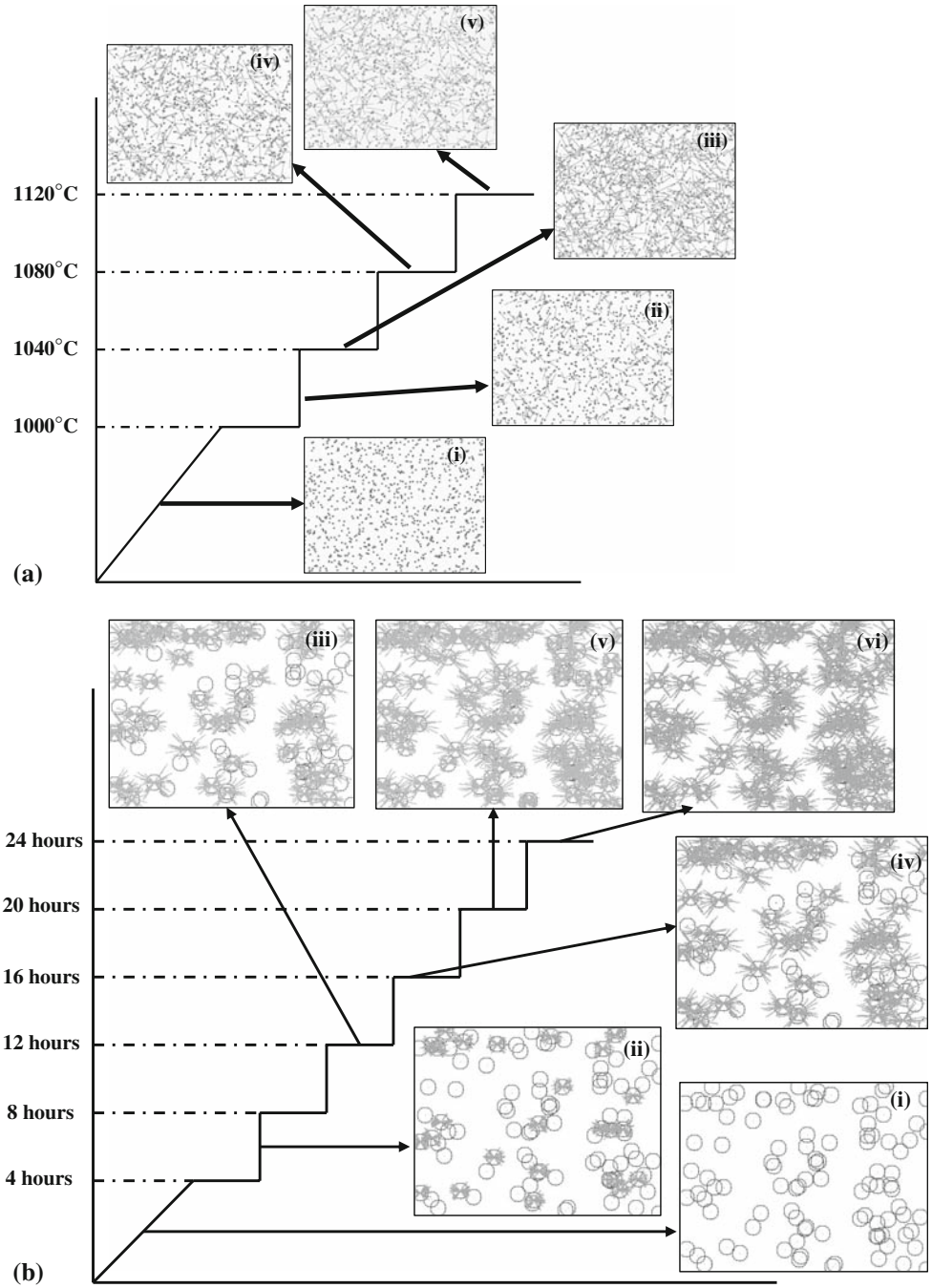

Fig. 9 Schematic representation illustrating the different stages of the microstructure development with possible crystal morphology formation of Flurophlogopite crystals from norbegite phase during heat treatment experiments (**a**) at constant time of 4 h for varying temperature intervals: (i) fragments of primary norbegite crystal phase scattered all over the sample; no detectable bulk crystal formation, (ii) FPP starts forming above 1,000°C in the bulk of the sample, (iii) maximum volume fraction of FPP formation at 1,040°C, (iv) and (v) FPP crystals with smaller aspect ratio dissolves and produces larger crystals at and above 1,080°C; crystal volume fraction decreases in the process, and (**b**) at constant temperature of 1,000°C for varying time intervals: (i) fragments of primary norbegite crystal phase scattered all over the sample, (ii) butterfly crystals tend to form from the initial norbegite crystals at holding time greater than 4 h, (iii), (iv) and (v) more and more butterfly crystals form with increasing holding time; volume fraction of crystalline phase increases; crystals start overlapping each other, and (vi) maximum crystal volume fraction obtained at holding time of 24 h; the whole sample is almost covered with butterfly crystals

ratio of crystals and restricts the maximum crystal formation within a limit of ~55% by volume [30]. In contrast, no such restricting mechanisms operates for the "spherulitic-dendritic" shaped crystals and therefore increased holding time manifests itself only in increased amount of crystallization.

Based on the above understanding, a schematic representation to illustrate the development of the spherulitic-dendritic like crystal morphology is presented in Fig. 10. The small scale perturbation at the interface of nucleus of crystalline phase and unvitrified glass matrix leads to the growth of the dendritic morphology, similar to that in metallic alloys. In Fig. 10, the development of longer primary arms as well as the secondary arms/side branches, inclined to an angle to the primary arm is also shown. The diffusion fields around the tip of both primary and secondary arms are shown. When the volume fraction of the crystals is high, then it is possible that diffusion fields of two primary arms, growing towards each other, will overlap and this will lead to the phenomenon of 'growth to impingement'. Similar situation also holds true for the branched secondary arms. Although a few secondary arms

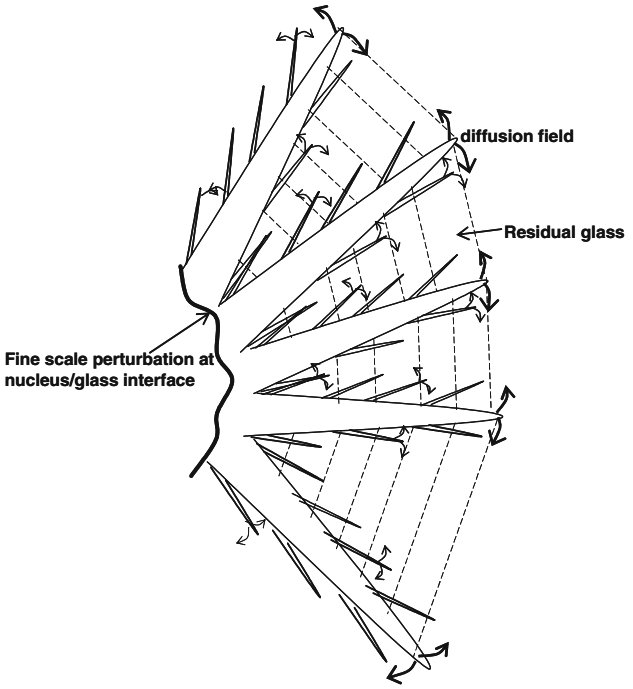

Fig. 10 Schematic representation to illustrate the development of the spherulitic-dendritic like crystal morphology, when SiO_2–MgO–Al_2O_3–K_2O–B_2O_3–F glass-ceramic is heat treated at 1,000°C for 8 h or longer. For symmetry, only a part of the characteristic crystal shape is shown and also the presence of residual glass phase in the intermediate region between two primary dendritic arms, is over emphasized. The diffusion to residual glass phase from the tip of dendritic arms (both primary and secondary) is also shown by arrows

are shown, they are much dense in numbers, as has been seen in our experiments. It needs to be realized the presence of a large number of secondary arms lead to what has been described earlier as 'tree leaves' structure. During the crystal growth process, the solute or part of the growing crystal composition is rejected to the residual glass phase in the neighborhood and such phenomenon establishes the requirement of the compositional undercooling for crystal growth.

4.2 Comparative mechanical and biological properties

In view of the potential engineering applications, the mechanical properties in terms of the scratch resistance as well as the in vitro dissolution properties of the two different crystal morphology ('spherulitic-dendritic and straw like crystals) were investigated and reported elsewhere in details [19–21]. While the scratch resistance has relevance to machining applications, the biological properties in terms of in vitro dissolution is of immense interest, considering the potential as dental prosthesis. As an addendum to the present work, we discuss below some illustrative evidences.

Scratch tests at a high load of 50 N can very well simulate the crack-microstructure interaction during real-time

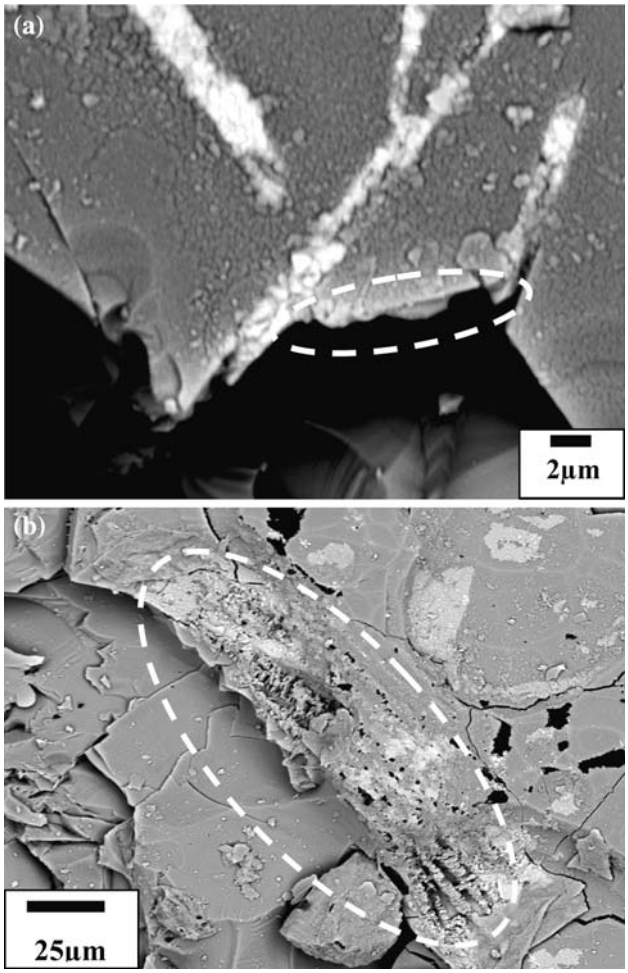

Fig. 11 SEM images revealing the interaction of the scratch induced crack with "straw" like crystals (bright contrast phase) in the mica based glass-ceramic sample (heat treated at 1,120°C for 4 h) leading to the crack deflection along the weak glass/crystal interface and subsequent spalling/pull-out of the glass matrix (shown with dotted line) (**a**). Similar interaction with "spherulitic-dendritic" shaped crystals in the sample (heat treated at 1,000°C for 16 h) leading to less severe damage, as evidenced by the absence of any significant spalling around stretched track (shown with dotted line) (**b**)

abrasion wear and machining operations. The experimental observations indicate that the novel "spherulitic-dendritic" shaped crystals, similar to the 'straw' like crystals, have the potential to hinder the scratching induced crack propagation (see Fig. 11). In particular, such potential of the 'spherulitic-dendritic' crystals become more effective due to the larger interfacial area with the glass matrix as well as the dendritic structure of each mica rod, which helps in crack deflection and crack blunting, to a larger extent. While layering of damage tolerant behavior is observed in case of 'spherulitic-dendritic' crystal containing material, severe brittle fracture of 'straw' like crystals were noted, when both were scratched at 50 N load.

Based on the experimental results obtained with the in vitro dissolution tests with SiO_2–MgO–Al_2O_3–K_2O–B_2O_3–

F glass ceramics, very minimal/insignificant weight loss as well as density variation are measured with the selected glass-ceramic samples, after 6 weeks of in vitro dissolution in artificial saliva solution (not shown here). Also, for the investigated glass-ceramics, a moderate bioactive behavior is observed. The presence of (Ca, P,O)-rich deposits on the leached surface as well as the Ca^{+2} ion concentration profiles of leaching solution provide evidences for mild bio-mineralization of both 'straw' and 'spherulitic-dendritic' crystals containing glass-ceramics. No observable change in shape of 'spherulitic-dendritic' crystals is observed after in vitro dissolution.

In summary, we have been able to demonstrate that new 'spherulitic-dendritic' crystal morphology in the SiO_2–MgO–Al_2O_3–K_2O–B_2O_3–F glass-ceramic system can be evolved during controlled heat treatment at 1,000°C. Also, very high volume fraction, up to around 70%, of crystalline phase can be formed after heat treatment for 24 h at 1,000°C. It can be noted that earlier studies reported the formation of a maximum of 50–55% crystalline phase with the usual 'straw' like crystals. Also, the formation of large amount of crystalline phase would improve the mechanical hardness and strength (machining applications) as well as in-vitro properties (dental restoration applications).

5 Conclusions

(a) The present study demonstrates that 'spherulitic-dendritic' crystal morphology, in contrast to commonly reported 'straw-like'/'house-of-cards' microstructure, develops during the single stage crystallization heat treatment of SiO_2–MgO–Al_2O_3–K_2O–B_2O_3–F glass at 1,000°C for 8–24 h.

(b) Both FT-IR and XRD analysis of the bulk glass-ceramic samples confirms the predominant presence of fluorophlogopite crystals phase in both temperature and time variation batches. However, no detectable crystal phase formation is observed after heat treatment at 1,000°C for 4 h. A longer incubation time of crystallization is consistent with our analytical calculation of kinetic parameters for crystallization, which reveals higher activation energy of 388 KJ/mol. Also, the diffusional growth could be justified by low Avrami index of 1.3.

(c) The crystallization behavior, in terms of morphology and amount of crystals, has been found to be strikingly different, depending on the heat treatment conditions. For heat treatment experiments with varying temperature (1,000–1,120°C), the volume fraction of crystalline phase varies around 45–58% with highest amount measured for samples heat treated at 1,040°C for 4 h. In contrast, for heat treatment at 1,000°C for varying time of 8–24 h, a systematic increase in volume fraction (up to 70%) with holding time is recorded. Additionally, DTA analysis indicates that the crystallization of this glass-ceramic system takes place in the temperature range of 732–962°C.

(d) The microstructural studies of temperature variation batches reveals the usual randomly oriented, interlocked 'straw' like mica plates; whereas time variation batches shows an unique 'spherulitic-dendritic' shaped morphology of the crystal phase, which is found to increase in number and overlap eventually as the holding time increases. The mica rods are observed to radiate from the initial norbergite nucleus with the end of each rod having a characteristic 'tree leaves' like feature and formed by stacking of mica plates. The growth of a large number of mica rods, resembling dendritic growth pattern, has been discussed in terms of radial chemical supersaturation from the primary nucleus, formed at multiple places during isothermal heat treatment.

(e) Based on the microstructural observations, a phenomenological model is proposed. The difference in two distinctly different morphologies is believed to be caused by the difference in the crystallization mechanisms of mica. The anisotropic growth dominates for temperature variation batches, whereas epitaxial growth in certain crystallographic directions other than the most preferable, in addition to the dendritic growth phenomena are likely to be the dominant mechanisms for crystallization of the newly reported 'spherulitic-dendritic' crystal morphology.

References

1. K. Lambrinou, J. Vleugels, A.R. Boccaccini, Formation of a metastable Celsian-Cordierite eutectic structure during the crystallization of a Ba-osumilite glass-ceramic. J. Am. Ceram. Soc. **90**(2), 590–597 (2007). doi:10.1111/j.1551-2916.2006.01430.x
2. A. Karamanov, M. Pelino, Evaluation of the degree of crystallization in glass-ceramics by density measurements. J. Eur. Ceram. Soc. **19**, 649–654 (1999). doi:10.1016/S0955-2219(98)00226-X
3. L.L. Hench, R.J. Splinter, W.C. Allen, T.K. Greenlee Jr., Bonding mechanisms at the interface of ceramic prosthetic materials. J. Biomed. Mater. Res. **5**(6), 117–141 (1971). doi:10.1002/jbm.820050611
4. W. Vogel, W. Höland, K. Kaumann, Development of machinable bioactive glass-ceramics for medical uses. J. Non-Cryst. Solids **80**, 34–51 (1986). doi:10.1016/0022-3093(86)90377-7
5. T. Höche, S. Habelitz, I.I. Khoodos, Origin of unusual fluorophlogopite morphology in mica glass-ceramics of the system SiO_2–Al_2O_3–MgO–K_2O–Na_2O–F_2. J. Cryst. Growth **192**, 185–195 (1998). doi:10.1016/S0022-0248(98)00458-8
6. Z. Hu, Y. Wang, F. Bao, W. Luo, Crystallization behavior and microstructure investigations on LaF_3 containing oxyfluride glass-ceramics. J. Non-Cryst. Solids **351**, 722–728 (2005). doi:10.1016/j.jnoncrysol.2005.01.075

7. S. Agathopoulos, D.U. Tulyaganov, P. Valerio, J.M.F. Ferreira, A new model formulation of the SiO_2–Al_2O_3–B_2O_3–MgO–CaO–Na_2O–F glass-ceramics. Biomaterials **26**, 2255–2264 (2005). doi:10.1016/j.biomaterials.2004.07.030
8. K. Cheng, J. Wan, K. Liang, Crystallization of R_2O–MgO–Al_2O_3–B_2O_3–SiO_2–F (R = K + , Na +) glasses with different fluorine sources. Mater. Lett. **47**, 1–6 (2001). doi:10.1016/S0167-577X(00)00201-9
9. T. Hoche, S. Habelitz, I. Avramov, Crystal morphology engineering in SiO_2–Al_2O_3–MgO–K_2O–Na_2O–F^- mica glass-ceramics. Acta Mater. **PII**, S1359–6454, 00424–8 (1998)
10. A. Gebhardt, T. Hoche, G. Carl, I.I. Khodos, TEM study on the origin of cabbage-shaped mica crystal aggregates in machinable glass-ceramics. Acta Mater. **47**(17), 4427–4434 (1999). doi:10.1016/S1359-6454(99)00317-1
11. A. Guedes, A.M.P. Pinto, M. Vieira, F. Viana, Multilayered interface in Ti:Macor® machinable glass-ceramic joints. Mater. Sci. Eng. A **301**, 118–124 (2001). doi:10.1016/S0921-5093(00)01804-9
12. P. Wange, T. Höche, T.C. Rüssel, J.D. Schnapp, Microstructure-property relationship in high-strength MgO–Al_2O_3–SiO_2–TiO_2 glass-ceramics. J. Non-Cryst. Solids **298**, 137–145 (2002). doi:10.1016/S0022-3093(02)00950-X
13. S.C. Clausbruch, M. Schweiger, W. Höland, V. Rheinberger, The effect of P_2O_5 on the crystallization and microstructure of glass-ceramics in the SiO_2–Li_2O–K_2O–ZnO–P_2O_5 system. J. Non-Cryst. Solids **263–264**, 388–394 (2000)
14. S. Taruta, K. Mukoyama, S·S. Suzuki, K. Kitajima, N. Takusagawa, Crystallization process and some properties of calcium mica-apatite glass-ceramics. J Non-Cryst. Solids **296**(3), 201–211 (2001). doi:10.1016/S0022-3093(01)00909-7
15. X. Chen, L.L. Hench, D. Greenspan, J. Zhong, X. Zhang, Investigation on phase separation, nucleation and crystallization in bioactive glass-ceramics containing fluorophlogopite and fluorapatite. Ceram. Int. **24**, 401–410 (1998). doi:10.1016/S0272-8842(97)00028-X
16. Y. Zhang, J.D. Santos, Crystallization and microstructure analysis of calcium phosphate-based glass-ceramics for biomedical applications. J. Non-Cryst. Solids **272**, 14–21 (2000). doi:10.1016/S0022-3093(00)00115-0
17. V.S. Nagrajan, S. Jahanmir, The relationship between microstructure and wear of mica-containing glass-ceramics. Wear **200**, 176–185 (1996). doi:10.1016/S0043-1648(96)07304-8
18. L. Radonjic, L. Nikalic, The effect of fluorine source and concentration on the crystallization of machinable glass-ceramics. J. Eur. Ceram. Soc. **7**, 11–16 (1991). doi:10.1016/0955-2219(91)90047-4
19. S. Roy, Microstructure development and in-vitro properties of macor glass-ceramics, Masters Dissertation, IIT Kanpur, India (2005)
20. S. Roy, B. Basu, Hardness properties and microscopic investigation of crack-crystal interaction in SiO_2–MgO–Al_2O_3–K_2O–B_2O_3–F glass ceramic system. Submitted to Mater. Sci. Eng. C (present status: under review)
21. S. Roy, B. Basu, In vitro dissolution behavior of SiO_2–MgO–Al_2O_3–K_2O–B_2O_3–F glass-ceramic system. J. Mater. Sci. Mater. Med. **19**(9), 3123–3133 (2008). doi:10.1007/s10856-008-3440-3
22. M.S. Bapna, H.J. Mueller, Study of devitrification of Dicer® glass. Biomaterials **17**, 2045–2052 (1996). doi:10.1016/0142-9612(96)00024-5
23. S. Habelitz, T. Höche, R. Hergt, G. Carl, C. Russel, Microstructural design through epitaxial growth in extruded mica glass-ceramics. Acta Mater. **47**(9), 2831–2840 (1999). doi:10.1016/S1359-6454(99)00135-4
24. W. Höland, Biocompatible and bioactive glass-ceramics—state of the art and new directions. J. Non-Cryst. Solids **219**, 192–197 (1997). doi:10.1016/S0022-3093(97)00329-3
25. D.R. Uhlmann, in *Advances in Nucleation and Crystallization in Glasses, Special Publication 5*, ed. by L.L. Hench, F. W. Freiman (American Ceramic Society, Columbus, 1971), pp. 91–115
26. W.A. Johnson, R.F. Mehl, Reaction kinetics in process of nucleation and growth. Trans. AIME **135**, 416–442 (1939)
27. M. Avrami, Kinetics of phase change, J. Chem. Phys. **7**, 1103–1112 (1939); **9**, 177–184 (1941)
28. J.W. Christian, *The Theory of Transformation in Metals and Alloys*, 2nd edn. (Pergamon Press, New York, 1975), p. 452
29. D.C. Clupper, L.L. Hench, Biomaterials **318**, 43–48 (2003)
30. W. Holand, G. Beall, *Glass-Ceramic Technology* (The American Ceramic Society, OH, 2002)
31. W. Holand, K. Zlateva, W. Vogel, I. Gutzow, Kinetic der phasesbidung in phologopit glass keramiken. Z. Chem. **22**, 197–202 (1982)
32. L. Lefebvre, J. Chevalier, L. Gremillard, R. Zenati, G. Thollet, D. Bernache-Assolant et al., Structural transformations of bioactive glass 45S5 with thermal treatments. Acta Mater. **55**, 3305–3313 (2007). doi:10.1016/j.actamat.2007.01.029
33. J. Henry, R.G. Hill, The influence of Lithia content on the properties of fluorphlogopite glass-ceramics. II. Microstructure hardness and Machinability. J. Non-Cryst. Solids **319**, 13–30 (2003). doi:10.1016/S0022-3093(02)01959-2
34. D.G. Grossman, Machinable glass-ceramics based on tetrasilicic mica. J. Am. Ceram. Soc. **55**(9), 446–449 (1972). doi:10.1111/j.1151-2916.1972.tb11337.x
35. R.E. Reed-Hill, *Physical Metallurgy Principles* (East-West Press Pvt. Ltd., New Delhi, 1974)
36. I. Gutzow, D. Kashchiev, I. Avramov, Nucleation and crystallization in glass-forming melts: old problems and new questions. J. Non-Cryst. Solids **73**, 477–499 (1985)
37. I. Avramov, The role of stress development and relaxation on crystal growth in glass. J. Non-Cryst. Solids **353**(30–31), 2889–2892 (2007). doi:10.1016/j.jnoncrysol.2007.06.008